X001

Seismic Scanning Tunneling Macroscope - Theory

G.T. Schuster* (King Abdullah University of Science & Technology), S.M. Hanafy (King Abdullah University of Science & Technology) & Y. Huang (King Abdullah University of Science & Technology)

SUMMARY

We propose a seismic scanning tunneling macroscope (SSTM) that can detect and distinguish sub-wavelength scatterers in the near-field of either the source or the receivers. Analytic formulas for the time reverse mirror (TRM) profile associated with a single scatterer model show that the spatial resolution limit to be, unlike the Abbe limit of λ/2, independent of wavelength and linearly proportional to the source-scatterer separation as long as the scatterer is in the near-field region. This means that, as the scatterer approaches the source, spatial imaging with super-resolution can be achieved. This is analogous to an optical scanning tunneling microscope that has sub-wavelength resolution. Scaled to seismic frequencies, it is theoretically possible to extract 100 Hz information from 20 Hz data by imaging of near-field seismic energy.

Introduction

Recently, Cao et al. (2011) used TRMs to locate trapped miners. They exploited the high-resolution and super-stacking properties of TRMs, but did not attribute this property to evanescent waves. Moreover, they only used the TRM methodology to locate trapped miners, not to characterize the distribution of scatterers in the earth.

This article shows both theoretically and experimentally that it is possible to use far-field seismic energy for sub-wavelength detection of sub-wavelength scatterers at seismic frequencies. The key idea is that seismic energy scattered from sub-wavelength objects located in the near-field of the source or receiver can be refocused with sub-wavelength resolution by TRM to the source location. This is similar to optical imaging devices that include a super lens in the near-field of the source (i.e., within a half-wavelength distance) that converts the evanescent energy to propagating waves (de Fornel 2001; Lerosey et al. 2007; Fink 2006). Analogous to the STM we propose a seismic scanning tunneling macroscope (SSTM) that can harness the sub-wavelength imaging potential in near-field seismic energy.

Seismic Scanning Tunneling Macroscope

Our proposed seismic scanning tunneling macroscope shares the same principle as the scanning tunneling microscope (STM) in producing images with high spatial resolution: small near-field changes in the separation of the source-object lead to enormous changes in the measured field. In the case of the STM, the measured field is the current at the scanning tip and for the SSTM it is the amplitude changes in the scattered field.

Figure 1a illustrates this idea for the STM (Binnig and Rohrer 1986; Bai 2000) where a conducting tip (a few atoms in width) is placed within a few Angstroms from the conducting surface of the object. The goal is to map out the topography of the conducting surface to within a few Angstroms of resolution. If the object is within the near-field of the tip, electrons can tunnel through the vacuum gap to create a current between the tip and object. This near-field current measured at the tip is very sensitive to slight changes in the height of the surface, as illustrated by the I(h) vs h plot on the right. Consequently, scanning the tip just above the surface (i.e., in the near-field region of the object's surface) can map out the surface topography to within a few nanometers. If the tip is too far away from the surface, i.e. the farfield region, then current fluctuations due to topography variations are too weak to be reliably measured. Analogously, the seismic scanning tunneling macroscope illustrated in Figure 1b relies on the fact that the scattered seismic energy from a sub-wavelength scatterer is very sensitive to the changes in the near-field separation r between the source and scatterer. This is caused by the strong sensitivity of the geometric spreading term 1/r to small near-field variations in the source-scatterer separation r (see Amplitude vs h curve in Figure 1b). We can also say that, the evanescent wave from the source converts to a propagating body wave at the scatterer that is recorded by the receivers (see Figure 2).

To utilize the evanescent energy in seismic waves, a sub-wavelength scatterer should be located in the near-field of the point source as shown in Figure 2. In the earth, scatterers can be small boulders buried near the source location. Here, the point source is located at $\mathbf{s}=(0,0)$ and is embedded in a homogeneous elastic medium with a near-field point scatterer at $\mathbf{s_0}=(0,\varepsilon)$; and the pressure field data are recorded along the line of receivers at $\mathbf{g}=(x_g,z_g)$ in Figure 2 that can be in the far-field of source. To understand the properties of imaging this point scatterer by a TRM we first derive its point scatterer response function.

Point Scatterer Response of the Near-field TRM Operator

Assume scattered data generated by a harmonic point source located at $\mathbf{s}$ and a scatterer at $\mathbf{s_0}$:

$$\boldsymbol{s\epsilon B_s; g\epsilon B_g;} \qquad G(\boldsymbol{g}|\boldsymbol{s})^{\boldsymbol{scatt.}} = G(\boldsymbol{g}|\boldsymbol{s_0})\boldsymbol{G}(\boldsymbol{s_0}|\boldsymbol{s}) \qquad (1)$$

where the scattering coefficient of 1 is conveniently assumed and G(**x**|**x'**) is the Green's function that solves the Helmholtz equation for a point source at **x'** and a receiver at **x** in a background velocity model. For mathematical convenience we assume an acoustic medium with the understanding that this procedure is applicable to an elastic medium. For a band-limited point source at **s**' with wavelet spectrum W(ω), the TRM image of the point source at **s**'ϵB_s for a continuous distribution of geophones along B_g is given by

$$s'\epsilon B_s \quad m(\boldsymbol{s'}) = \int_{-\omega_0}^{\omega_0}\int_{-L}^{L} k|W(\omega)|^2\, G(\boldsymbol{g}|\boldsymbol{s_0})G(\boldsymbol{s_0}|\boldsymbol{s})G^*(\boldsymbol{g}|\boldsymbol{s_0})G^*(\boldsymbol{s_0}|\boldsymbol{s'})d\boldsymbol{g}d\omega \qquad (2)$$

If the background medium is homogeneous with velocity c, the background Green's function takes the form $G(\boldsymbol{x}|\boldsymbol{x'}) = \frac{e^{i\omega|x-x'|/c}}{|x-x'|}$, where k=ω/c. The frequency band of the flat source spectrum is between -ω_0 and ω_0, and the recording aperture is 2L wide. The extrapolator ($G^*(\boldsymbol{g}|\boldsymbol{s_0})G^*(\boldsymbol{s_0}|\boldsymbol{s'})$) plays the role of focusing the recorded energy back to the trial source location at **s**'.

For convenience, assume $|W(\omega)|^2=1/k$ so that plugging the background Green's function into Equation (2) gives

$$m(\boldsymbol{s'}) = \int_{-\omega_0}^{\omega_0} \frac{e^{i\omega(|s_0-s|-|s_0-s'|)/c}}{|s_0-s|-|s_0-s'|}d\omega \int_{-L}^{L}\frac{1}{|g-s_0|^2}\boldsymbol{dg}, = \frac{\alpha(\boldsymbol{s},\boldsymbol{s_0},\boldsymbol{s'})\sin(\frac{\omega_0\left[|\boldsymbol{s_0}-\boldsymbol{s}|-|\boldsymbol{s_0}-\boldsymbol{s'}|\right]}{c})}{\left[|\boldsymbol{s_0}-\boldsymbol{s}|-|\boldsymbol{s_0}-\boldsymbol{s'}|\right]}, \qquad (3)$$

where the near-field geometrical spreading factor α(**s**,**s**$_0$,**s'**) is defined to be

$$\alpha(\boldsymbol{s},\boldsymbol{s_0},\boldsymbol{s'}) = \frac{c}{[|s-s_0|-|s'-s_0|]}\int_{-L}^{L}\frac{1}{|g-s_0|^2}d\boldsymbol{g}.$$

Equation (3) is used to compute the TRM profile for the trial source positions **s**' along a specified line that intersects the actual source position at **s**.

The first zero-crossing of m(**s**') is given by **s**' that satisfies $\gamma = [|\boldsymbol{s_0}-\boldsymbol{s}|-|\boldsymbol{s_0}-\boldsymbol{s'}|] = \frac{-\boldsymbol{\lambda_0}}{\boldsymbol{2}}$, and, under the traditional Rayleigh resolution criterion, determines the spatial resolution of the imaged source location; here $\lambda_0=2\pi c/\omega_0$.

For the scatterer at **s**$_0$=(0,ε), the source at **s**=(0,0), and **s**'=(x',0), γ becomes $\gamma = \left[\boldsymbol{\varepsilon}-\sqrt{\boldsymbol{\varepsilon^2}+\boldsymbol{x'^2}}\right] = \frac{-\boldsymbol{\lambda_0}}{\boldsymbol{2}}$. For ε≈ 0 the first zero-crossing is at $x' = \lambda_0/2$, which is the Abbe limit and the sinc-like function is illustrated by the solid-line curves in Figure 3. As expected, the sinc-like function widens as the point scatterer is moved further away from the point source.

However, the first zero-crossing is not the only determinant of the spatial resolution limit Δx because the near-field geometrical spreading factor α(**s**,**s**$_0$,**s'**) is proportional to $\frac{1}{|s'-s_0|}$, which spikes the central part of the sinc function for small ε and $|\boldsymbol{s'}-\boldsymbol{s_0}|$. This spiking is illustrated by the dashed-line curves in Figure 3, where the half-width of $\frac{1}{|s'-s_0|}$ is $\boldsymbol{\Delta x'} = \boldsymbol{\beta\varepsilon}$. Consequently, the near-field horizontal resolution becomes better as the point scatterer approaches the source position. Here, β is a constant that depends on the type of resolution criterion and is equal to 2 if a half-power criterion is used. In the Figure 3 example, the dominant wavelength of the transient source is 120 m. Beyond the source-scatterer distance of about λ/2 the sinc-like function determines the horizontal resolution limit (i.e., Abbe), otherwise it is controlled by the inverse-distance function to yield sub-wavelength resolution.

The near-field resolution limit says that the evanescent energy introduces an effective horizontal wavelength that is linearly proportional to the distance between the scatterer and the point source.

And for source-scatterer separations greater than λ/2 the sinc-like function controls lateral resolution, not the near-field geometrical spreading factor in Equation (4).

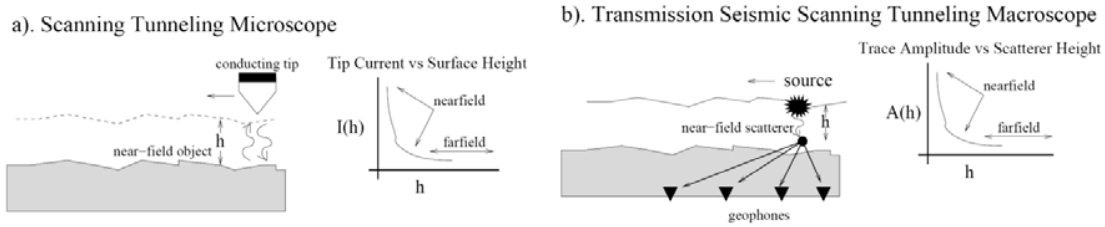

Figure 1 *Illustration of a) Scanning Tunneling Microscope (STM) and b) transmission Seismic Scanning Tunneling Macroscope. In the STM (SSTM) example, small changes in the source-object (source-scatterer) separation lead to enormous changes in the measured current (trace amplitude of scattered energy) measured at the tip (geophone). It is assumed that both the tip (seismic source) and object (seismic scatterer) are sub-wavelength in dimension and are separated by less than λ/2. A key difference between the STM and SSTM is that the SSTM receivers can be in the far-field of the scatterer.*

Synthetic Data Tests

Synthetic data are used to test for sub-wavelength resolution by the SSTM, where an acoustic Born modeling procedure with ray tracing is used to generate the scattered data. Figure 4a depicts a shot gather of scattered arrivals for the two scatterer model in Figure 4b with a source at (60,0) m. Here, the scatterers are separated by 10 m and located 5.2 m from the source line at z=0. These data are recorded 45 m above the source line and are used to create the TRM profile in Figure 4c; here, the TRM profile clearly distinguishes the separation of the two scatterers from one another, despite the 100 m wavelength. The horizontal resolution of this scattered wave TRM profile is approximately λ/20. In contrast, the TRM profile associated with the direct wave in Figure 4d is diffraction limited.

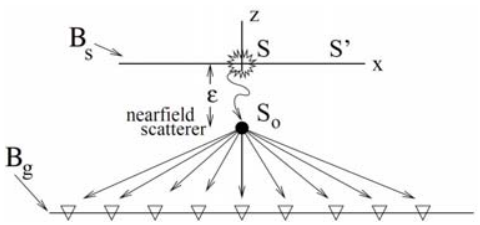

Figure 2 *Single scatterer in the near-field of the source and the geophones are in the farfield region. The horizontal resolution limit of the source image is proportional to ε for a homogeneous background medium.*

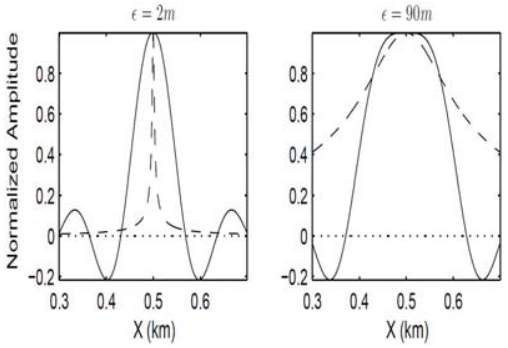

Figure 3 *Plots of sinc-like function (solid lines) in Equation (3) and inverse-distance function (dashed lines) in $\alpha(\boldsymbol{s}, \boldsymbol{s_0}, \boldsymbol{s'})$ for a point scatterer 2 m (left plot) and 90 m (right plot) from the point source.*

Conclusions

The theory for a SSTM is proposed and validated with synthetic data. OUR companion EAGE abstract confirms that super-resolution is valid with elastic data, both for simulations and for field data

tests. The key assumptions are that there are sub-wavelength scatterers in the near-field of the source, the geophones can be in the far-field of the source, and scattered energy can be separated from the strong direct arrivals. Synthetic tests validate this claim and results for Arizona tunnel data are presented in our companion EAGE abstract.

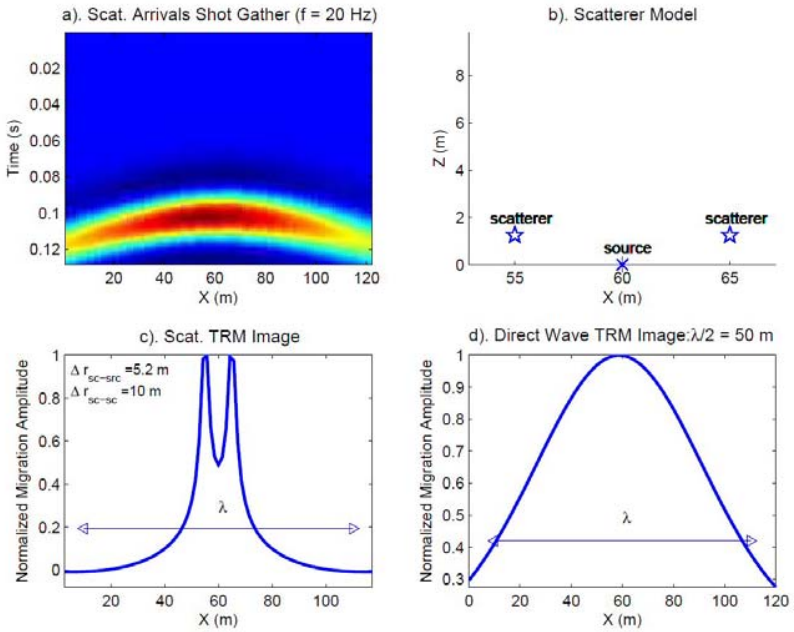

Figure 4 *a). Shot gather for the two-scatterer model in b), where the point source is at (x,z)=(60,0) m; here the far-field geophone positions are along a horizontal line 45 m above the horizontal source line. The scatterers are located in the near-field region of the source (5.2 m source-scatterer separation), where the wavelength of the source is 100 m. The TRM profile at z=0 for a source at* ***s****=(60,0) m using only scattered arrivals shows a horizontal resolution of approximately λ/20; here the horizontal axis indicates the trial source position* ***s'****. In contrast, the TRM profile using only the direct arrivals is in d) and shows diffraction-limited resolution.*

References

Bai, C. [2000] Scanning tunneling microscopy and its applications. New York: Springer Verlag. ISBN 3540657150.

Binnig, G. and Rohrer, H. [1986] Scanning tunneling microscopy. IBM Journal of Research and Development, **30**, 4.

Cao, W., Hanafy, Sh., Schuster, G.T., Zhan, G. And Boonyasiriwat, C. [2011] High-resolution and super-stacking of time reversal mirrors in locating seismic sources. Geophysical Prospecting, doi: 10.1111/j.1365-2478.2011.00957.x

de Fornel, F. [2001] Evanescent Waves from Newtonian Optics to Atomic Physics. Springer-Verlag.

Fink, M. [2006] Time-reversal acoustics in complex environments. Geophysics, 71, SI151-SI164.

Lerosey, G., de Rosny, J., Tourin, A., and Fink, M. [2007] Focusing beyond the diffraction limit with far-field time reversal. Science, **315**, 1120-1122.